Nonlinear hydrodynamics of a heaving sphere in diffraction, radiation, and combined tests

Jana Orszaghova, Hugh Wolgamot, Adi Kurniawan, Daniel Ho, Bryan Tan, Guy McCauley, and Jørgen Hals Todalshaug

Abstract—**We report on an experimental campaign designed to shed light on critical nonlinear hydrodynamic effects of heaving wave energy converter (WEC) buoys undergoing large-amplitude motions in operational conditions. The experiments carried out with a spherical model comprised radiation, diffraction and combined tests, where the vertical motion was prescribed and delivered via an actuator. As such, we had independent control of incident waves and motions, enabling isolation of different nonlinear terms by combining recordings from multiple phase- and amplitude-manipulated runs. All tests utilised short-duration wave groups and/or corresponding transient motion signals.**

We focus on analysis of nonlinear changes in the hydrodynamic forces, and free surface, in the first-harmonic frequency range - this is of most importance to WECs. In a series of radiation experiments, with progressively increasing imposed motions, the radiated wave field and the force in phase with the body velocity are found to decrease nonlinearly, pointing to the WEC's reduced ability to radiate waves under larger oscillations. In the combined tests, we are able to isolate various high-order cross-terms. We attempt to explain the observed trends through third-order potential flow interactions and consider a simple method to approximately describe these.

Index Terms—**wave energy, nonlinear hydrodynamic forces, amplitude dependence, radiation damping, third-order potential flow effects**

I. Introduction

WAVE-structure interactions have been studied extensively for fixed and floating offshore and coastal structures. Within the framework of potential flow theory, linear and second-order calculations are now widely used. Much emphasis has been on understanding and modelling nonlinearities arising from large incident waves. For floating structures, however, non-linear effects can also arise from large body motions. This is of much relevance to wave energy converters (WECs) designed to operate in resonance with the wavefield, and thus undergoing relatively large oscillations even in mild and moderate sea states.

Traditional offshore structures are designed with response natural frequencies outside the typical wave frequencies, in order to avoid resonance. Investigations of nonlinear effects have thus primarily focused on the super- and sub-harmonic frequency ranges. Superharmonic excitation, from second- and higher-order sum-frequency interactions, is of relevance to fixed structures [1], for example for the springing and ringing structural responses in monopiles. Sub-harmonic excitation, primarily from second-order difference-frequency interactions, is important for soft-moored floating structures, with regards to resonant slow-drift motions of vessels, floating productions and floating wind turbines [2] for example. Much less emphasis has been given to the study of nonlinear effects in the first-harmonic frequency range. This frequency region is of foremost importance to wave energy converters, which aim to extract maximum energy from these, main energy-bearing, incident wave components.

In this work we experimentally investigate nonlinear hydrodynamic forces on, and the associated wave field around, a heaving sphere in pure radiation tests as well as in the presence of incident waves. We utilise phase-manipulated focused wave groups, as well as phase-manipulated imposed body motions, in order to isolate different harmonics. We then analyse in detail the non-linear changes in the first-harmonic range as the motion amplitude is increased. A short theoretical background is provided in Section II. The experiments are described in Section III. Analysis of the measurements and results are discussed in Section IV. Finally, implications and conclusions are given in Section V.

II. Weakly nonlinear potential flow theory

Within weakly nonlinear potential flow theory framework, the wave-wave or wave-structure interaction solution, for free surface or other associated wavefield variables such as the hydrodynamic force for example, can be described as

$$\begin{aligned} C(t) = {} & A(t) f^{(1)} \cos(\phi + \theta^{(1)}) + \\ & A^2(t)\Big(f^{(2-)} + f^{(2+)} \cos(2\phi + \theta^{(2+)})\Big) + \\ & A^3(t)\Big(f^{(3-)} \cos(\phi + \theta^{(3-)}) + f^{(3+)} \cos(3\phi + \theta^{(3+)})\Big) + \\ & O(A^4), \end{aligned} \tag{1}$$

where $C(t)$ is the nonlinear quantity of interest, here shown as a function of time t. In the above, for the sake of conciseness, we have adopted a narrow-banded notation, where $A(t)\cos(\phi) = A(t)\cos(\omega t + p)$ represents the linear content of the incident waves, with $A(t)$ denoting the slowly-varying envelope, ω the peak frequency and p its phase. The linear and high-order

J. Orszaghova, H. Wolgamot, A. Kurniawan, D. Ho, B. Tan, G. McCauley are at the University of Western Australia, 35 Stirling Highway, 6009, Western Australia (e-mail: jana.orszaghova@uwa.edu.au, hugh.wolgamot@uwa.edu.au, adi.kurniawan@uwa.edu.au).

J.H. Todalshaug is with CorPower Ocean, Västberga Allé 60, 126 30 Hägersten, Sweden (e-mail: jorgen.hals@corpowerocean.com).

Digital Object Identifier:
https://doi.org/10.36688/ewtec-2023-474

transfer functions, described by amplitudes $f^{(n\pm)}$ and phases $\theta^{(n\pm)}$, are the frequency-dependent relations between the incident waves and the n^{th} harmonic of the response quantity of interest C. The equivalent expressions, without the simplified narrow-banded notation, can be found in [3] and [4] for example.

At second order, the quadratic transfer functions describe interactions between pairs of underlying frequency components. These can occur at difference and sum frequencies, and are termed sub- and superharmonics owing to the fact that they respectively span frequency ranges below and above the linear content. These are respectively denoted by superscripts $(2-)$ and $(2+)$ in equation 1. Second-order responses scale as a square of the incident waves.

At third order, the cubic transfer functions describe interactions between triplets of components. The superharmonic $(3+)$ terms arise from the so called $(++)$ sum-frequency interactions and are centered in frequency around 3ω. On the other hand, the $(3-)$ terms, representing the so called $(+\,+\,-)$ interactions, overlap with the first-harmonic range. Since they scale as a cube of the incident wave steepness in the perturbation expansion, their magnitudes are smaller than the linear terms. As such the $(3-)$ interactions have not been studied widely as, in general, linear theory adequately captures the dominant dynamics in this frequency range. Moreover, a complete third-order theory for wave-structure interactions has not been developed (see e.g. [5] for approximations). For WECs the first-harmonic range is of most relevance, and investigating nonlinear hydrodynamic effects at these frequencies is the main focus of our work.

For clarity in the remainder of the paper, we use the term 'first-harmonic' to denote all content in this frequency range, so both the linear (1) and the third-order $(3-)$ terms. We reserve the term 'linear' for referring to terms which scale linearly with amplitude A (and/or the motion amplitude X, which is introduced later).

We briefly comment on the nature and origin of the nonlinear interactions. At second order, when considering the hydrodynamic force as an example, one of the forcing terms originates from an integral of the linear hydrodynamic pressure calculated over the linear time-varying portions of the instantaneous submerged hull surface. If we consider only the linear incident and diffracted wavefields (including the associated linear runup on the body) but disregard the instantaneous body position, then the second-order interaction constitutes wave terms only. If we also considered the linear radiated waves and/or the linear body position, then we have additional wave-motion interaction terms, as well as motion-motion terms. We note in passing that in the full second-order theory (see e.g. [6] and [7]) there are other second-order terms in addition to the illustrative example discussed here. This description/classification can also be generalised to third order, with www, wwm, wmm and mmm terms arising, where we used w and m to denote the wave and motion variables respectively. In experiments where the waves and the body motions are controlled independently, unlike in tests with freely floating bodies, we can start to tease out the different nonlinear terms.

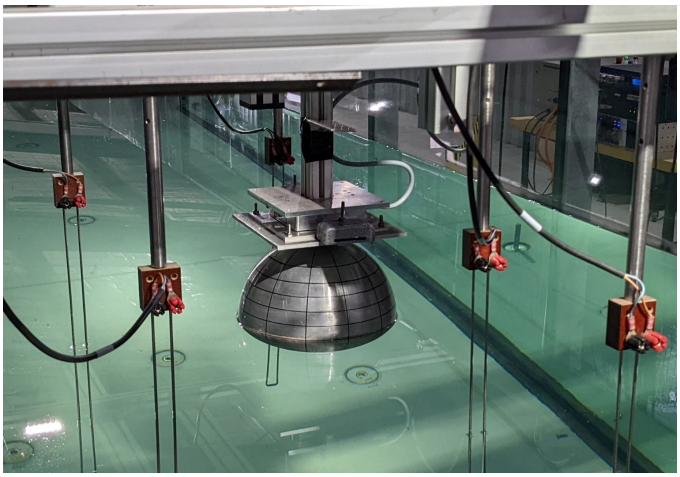

Fig. 1. Experimental setup. The spherical model can be seen in the middle of the photograph, with the load cell attached above, which is in turn rigidly connected to the vertical actuator arm. Five wave gauges can be seen in the model's proximity, while others were placed further up- and down-wave of the model.

III. Experimental details

The experiments were carried out in the 50 m long and 1.5 m wide wave flume at the Coastal and Offshore Engineering Laboratory at the University of Western Australia. Waves were generated by a hinged wavemaker on one end of the flume, and absorbed passively on a 1:10 sloping perforated beach at the other end. A 0.25 m diameter aluminium sphere was connected to a linear actuator, which either held the sphere fixed (diffraction tests) or oscillated the sphere vertically according to a prescribed motion command (radiation and combined tests). The achieved displacement was measured with a laser distance sensor as well as via an encoder in the actuator motor. A 3-axis 50 N load cell measured the total forces experienced by the model. The sphere was positioned along the flume centreline and approximately 10 m from the wavemaker. An array of resistance-type wave gauges was used to record the free surface in the vicinity of the model. Loads and displacements were logged at 100 Hz, while waves were recorded at 128 Hz. Two data acquisition systems were utilised and synchronisation across all data channels was ensured via a trigger signal common to both systems. Three high-speed cameras were used to capture the instantaneous runup on the sphere. Fig. 1 shows the experimental setup.

All tests utilised short-duration broad-banded wave groups and/or corresponding transient motion signals, to minimise issues with reflected waves from flume ends. A focused wave group is simply a superposition of different frequency components which are all in phase at a single location/time. The incident wave groups were derived from an underlying JONSWAP spectrum, with peak frequency $f_p = 0.8$ Hz and high-frequency cut-off at $2.5f_p$. The linear focus location was set to be the sphere centre. Both crest- and trough-focused wave group tests were carried out, with and without the model in place. The undisturbed free surface measurements from the sphere location were used

to create the displacement signals for the actuated tests - a universal phase shift and amplitude scaling was applied to all the first-harmonic wave components. The experimental campaign comprised over 200 tests, and the subset of tests analysed in this paper is summarised in Table I. Each test is characterised by the nominal linear focus amplitude and phase of the incident waves and the motions, with (A, p_w) defining the waves, and (X, p_m) the motions. Diffraction, radiation and combined tests are denoted by D, R and C respectively.

Independent control of the incident waves and the model motions allows for isolation of different linear and higher-order terms in the measured loads and free surface, by judiciously combining recordings from multiple phase- and amplitude-manipulated runs. This method was originated by [8] and can be viewed as an extension of two- and four-phase combination methods ([9] and [10] for example) in wave-structure interaction tests with a single controlled input (which is typically the incident wavefield in experiments with fixed or freely floating bodies). The following combinations of 4 combined tests allow us to separate the linear diffraction and the linear radiation terms, each also additionally accompanied by various third-order terms:

$$\begin{aligned}&\frac{1}{4}\Big(C_{(0,270)} + C_{(0,90)} - C_{(180,270)} - C_{(180,90)}\Big) = \\ &Af_w\cos(\phi+\theta_w)+ \\ &A^3\Big(f^-_{www}\cos(\phi+\theta^-_{www}) + f^+_{www}\cos(3\phi+\theta^+_{www})\Big)+ \\ &AX^2\Big(f^-_{wmm}\cos(2\psi-\phi+\theta^-_{wmm})+ \\ &\qquad f^+_{wmm}\cos(2\psi+\phi+\theta^+_{wmm})\Big) \\ &+O(A^5),\end{aligned} \tag{2}$$

$$\begin{aligned}&\frac{1}{4}\Big(C_{(0,270)} - C_{(0,90)} + C_{(180,270)} - C_{(180,90)}\Big) = \\ &Xf_m\cos(\psi+\theta_m)+ \\ &X^3\Big(f^-_{mmm}\cos(\psi+\theta^-_{mmm}) + f^+_{mmm}\cos(3\psi+\theta^+_{mmm})\Big)+ \\ &XA^2\Big(f^-_{mww}\cos(2\phi-\psi+\theta^-_{mww})+ \\ &\qquad f^+_{mww}\cos(2\phi+\psi+\theta^+_{mww})\Big) \\ &+O(A^5),\end{aligned} \tag{3}$$

where $C_{(p_w,p_m)}$ represents the measured nonlinear time series from a combined test with the prescribed motion given by $X\cos\psi = X\cos(\omega t + p_m)$ and the linear content of the incident waves given by $A\cos\phi = A\cos(\omega t + p_w)$. Note that we have omitted the explicit time dependence of A and X, and are using these symbols for envelopes and linear focus amplitudes interchangeably. As above, the transfer functions are defined by f and θ, and here we have explicitly written out the different nonlinear terms. Equations (2) and (3) are used to process groups of 4 combined tests (for example C1–C4 from Table I).

In the absence of body motions, when $X = 0$, equation (2) can be used to process pairs of diffraction tests (for example D1 and D2 from Table I):

$$\begin{aligned}&\frac{1}{2}\Big(D_0 - D_{180}\Big) = Af_w\cos(\phi+\theta_w)+ \\ &A^3\Big(f^-_{www}\cos(\phi+\theta^-_{www}) + f^+_{www}\cos(3\phi+\theta^+_{www})\Big)+ \\ &O(A^5).\end{aligned} \tag{4}$$

Similarly, in the absence of incident waves, when $A = 0$, equation (3) can be used to process pairs of radiation tests (for example R1 and R2 from Table I):

$$\begin{aligned}&\frac{1}{2}\Big(R_{270} - R_{90}\Big) = Xf_m\cos(\psi+\theta_m)+ \\ &X^3\Big(f^-_{mmm}\cos(\psi+\theta^-_{mmm}) + f^+_{mmm}\cos(3\psi+\theta^+_{mmm})\Big)+ \\ &O(X^5).\end{aligned} \tag{5}$$

Even though the equations might be lengthy, their application is straightforward - we simply subtract and/or add signals from pairs/quartets of synchronised runs. The key point to note about our testing campaign is that groups of tests were performed at different excitation levels (A and X), enabling explicit identification of amplitude scaling of the different nonlinear terms.

Lastly, in order to isolate the first-harmonic frequency content from (2)–(5), a low-pass filter is applied to remove the higher frequency terms around 3ω and beyond. The remaining components, however, contain both the linear and the $(3-)$ terms. We are interested in understanding the role of the $(3-)$ interactions and whether they have a marked effect as body motions and/or incident waves increase. The fact that the above equations contain only odd-order harmonic terms is key for clear separation as the first-harmonic and the third-order super-harmonics overlap minimally. For brevity, we have omitted the analogous equations for even-order harmonics.

IV. Analysis of first-harmonic forces and free surface

In this section, we present results of the analysis of the first-harmonic forces and free surface. We first process pairs of radiation runs, and then proceed onto combined runs. It is important to note that the measurements from the load cell represent the total force experienced by the sphere. In order to isolate the hydrodynamic force content, inertia and hydrostatic forces are removed first. These are calculated from the sphere mass and volume, and its displacement and acceleration recorded during each test. The remainder hydrodynamic force constitutes a small fraction of the total force, so accurate estimates of the mass and geometric properties of the model are important. In this work, we analyse the vertical force. Due to the symmetry of the setup, there is no transverse force, and the horizontal force in the incident wave direction arises in the diffraction and combined tests only.

A. Radiation tests

The measured vertical hydrodynamic force, in the first-harmonic frequency range, from the radiation runs is shown in Fig. 2. These signals follow from (5) and the application of a low-pass filter, as explained above. The force recording from the $X = 0.05$ m radiation runs is corrupted, so has been omitted. As expected, the force

TABLE I
SUMMARY OF TESTS ANALYSED

	X [m]	0	0.02	0.02	0.05	0.05	0.08	0.08	0.10	0.10
A [m]	p_w [°] \ p_m [°]	-	270	90	270	90	270	90	270	90
0	-		R1	R2	R3	R4	R5	R6	R7	R8
0.025	0	D1	C1	C2	C5	C6	C9	C10		
0.025	180	D2	C3	C4	C7	C8	C11	C12		

increases with the imposed motion amplitude. In all plots in this paper, apart from Fig. 8, blue, red, yellow and purple lines consistently refer to conditions with motion amplitudes X of 0.02, 0.05, 0.08 and 0.10 m respectively.

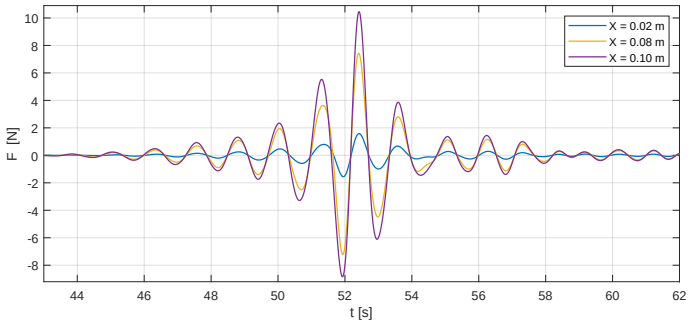

Fig. 2. First-harmonic hydrodynamic force from radiation runs.

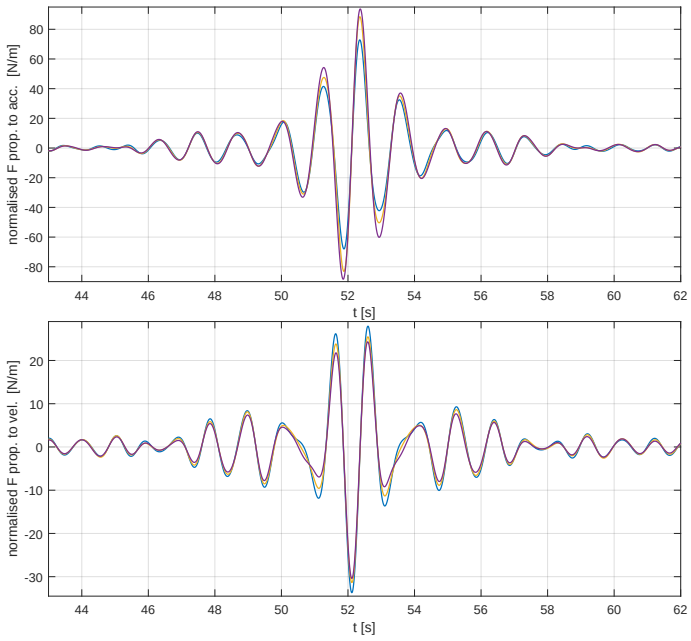

Fig. 3. Normalised first-harmonic radiation force components in phase with body acceleration (top) and in phase with body velocity (bottom).

We can split the radiation force into two components, in phase with the model acceleration and with the model velocity. Considering these are first-harmonic force components, we can normalise the signals by their respective imposed motion amplitude X. These are shown in Fig. 3. Around the largest crests and troughs in the signals, we note progressive deviations across the three signals - a sign of nonlinearity. The force component in phase with the body acceleration increases, while the component in phase with the body velocity decreases nonlinearly with the prescribed motion amplitudes. We also note that the total force is dominated by the component in phase with the body acceleration.

In the frequency domain, the same trend can be seen in the force transfer functions shown in Fig. 4 - added mass increases while radiation damping decreases. Data from the smallest motion test aligns with linear theory closest, while deviations become more pronounced for the larger imposed motion tests. The linear force coefficients are calculated by diffraction/radiation code Hydrostar [11]. We note the rather unusual shape of the transfer functions. The sharp peaks arise due to cross-modes in the flume. The even modes are of relevance here, whose wavelengths follow from $\lambda_n = W_F/n$, where W_F is the flume width and n an integer. The first two even modes are shown in the figure.

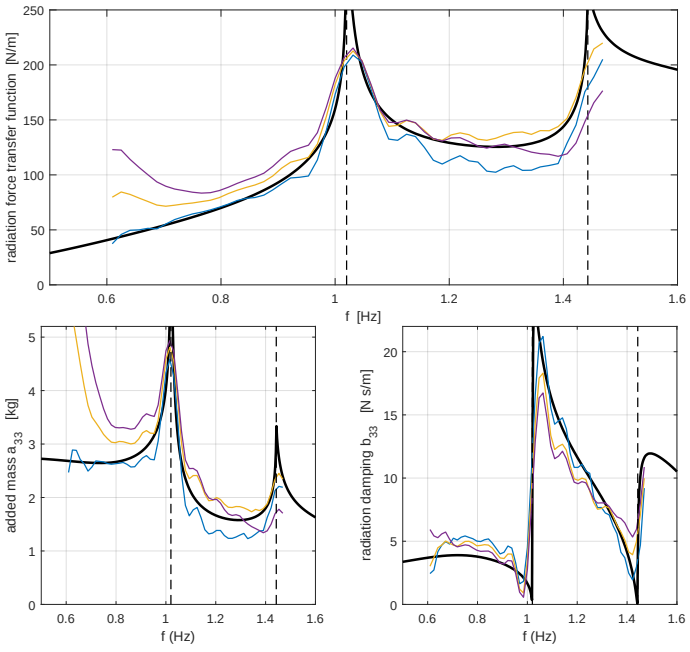

Fig. 4. Radiated force transfer functions. Linear solution shown in black solid line, and flume cross-mode frequencies shown by vertical dashed lines.

In order to investigate the nature of the nonlinearities observed, we recall that the extracted first-harmonic forces contain linear as well as third-order $(3-)$ mmm terms, as per (5). These terms can be separated through amplitude-manipulated tests as follows. Assuming that the smallest motion-amplitude first-harmonic force signal (from tests R1 & R2 with $X = 0.02$ m) is linear, we

can first scale it linearly to the other two cases (via multiplication by $\frac{8}{2}$ for tests R5 & R6 and via multiplication by $\frac{10}{2}$ for tests R7 & R8). We can subsequently deduct it from the first-harmonic force signals (from tests R5 & R6 and R7 & R8). The remainder should be the $(3-)$ mmm terms, which should scale as a cube of the imposed motion amplitudes. This is tested in Fig. 5, which shows the remainder signals normalised by X^3. The rather good collapse of the curves is a compelling demonstration that the nonlinear variation of the radiation forces in the first-harmonic frequency range can be interpreted as third-order interactions.

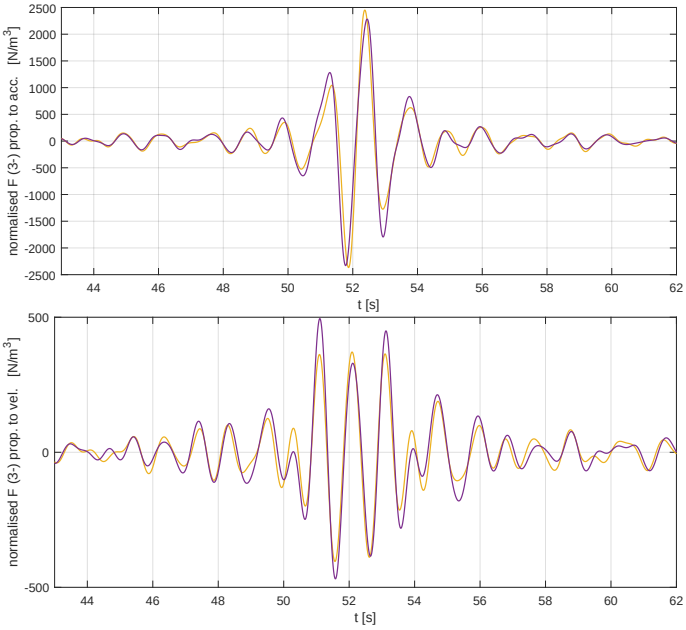

Fig. 5. Extracted normalised (3-) mmm radiation force components in phase with body acceleration (top) and in phase with body velocity (bottom).

We can supplement the above results for radiation forces with the free surface data. We first investigate the normalised first-harmonic wave data, as shown in Fig. 6. These plots are equivalent to Fig. 3, with the $X = 0.05$ m tests also included for which the force measurements were corrupted. The free surface can be seen to vary nonlinearly with the imposed motion amplitudes and exhibits a decreasing trend. We also note the long-lived nature of the radiated wavefield, persisting for times beyond the largest body motions. This is a consequence of the presence of the flume walls.

We proceed to test our hypothesis of third-order interactions. The normalised extracted $(3-)$ mmm free surface terms are shown in Fig. 7. Here, we have three curves, as we also use the free surface data from the $X = 0.05$ m radiation runs, for which the force data was not available. The collapse is reassuring.

From Figs. 3, 4 and 6, the observed decrease in both the normalised radiated free surface and the force component in phase with the body velocity are consistent as per linear theory where the radiation damping force is directly related to the propagating radiated wavefield. A simplified interpretation of the observations can be made in terms of the displaced volume of water

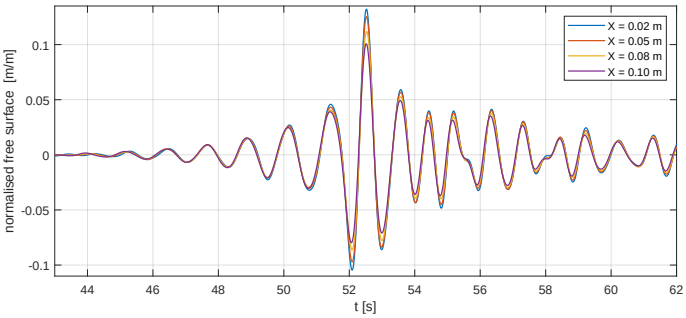

Fig. 6. Normalised first-harmonic radiated free surface. Data from wave gauge approximately 0.05 m behind the sphere is used.

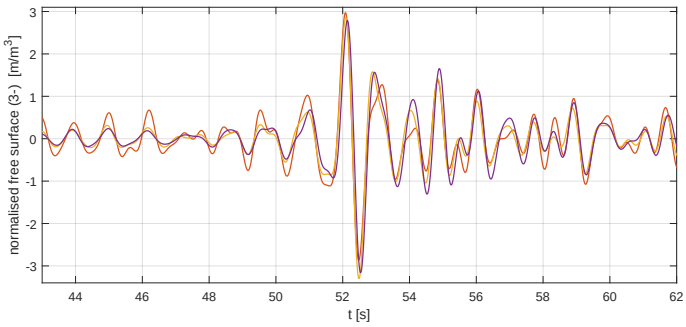

Fig. 7. Extracted normalised (3-) mmm radiated free surface components.

as the sphere oscillates. For a non-cylindrical geometry, the volume changes are nonlinear. It is perhaps not surprising that the wave-radiating ability of the model is progressively reduced at larger motion amplitudes. The volume considerations are of course not the only source of nonlinearity - we would expect deviations from linear theory also for cylindrical bodies undergoing large oscillations. Lastly, we comment on the variation of the radiated force proportional to body acceleration. These added-inertia effects would modify the heave natural frequency of the body under large oscillations, which in a heaving WEC could lead to detuning from resonant behaviour.

We return to the transfer function plots from Fig. 4. We can view the experimental curves as corrections to the linear theory, but it should be borne in mind that these are amplitude-dependent. For this reason, one cannot simply take the altered coefficients and apply them in linear calculations. An account of the nonlinear forcing has to be made. We will return to this later.

B. Combined tests

We now analyse the combined tests, processing quartets of tests as explained in Section III. We note that the incident wave conditions are kept the same across all tests described here. The imposed motions are the same as in the radiation runs, though the largest $X = 0.10$ m case was omitted in order to avoid wave runup reaching the top or the bottom of the sphere.

The extracted first-harmonic vertical hydrodynamic force remainder (once inertia and hydrostatic forces have been removed) is shown in Fig. 8. The combined tests are processed according to (2) and (3). We have also superimposed the corresponding force

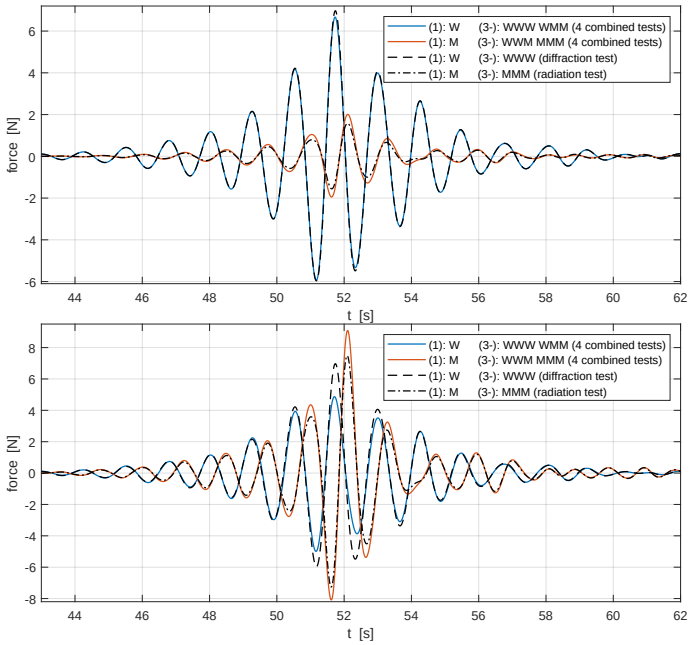

Fig. 8. First-harmonic hydrodynamic force from combined, radiation and diffraction runs. Top and bottom plots are for motion amplitudes of $X = 0.02$ m and $X = 0.08$ m cases respectively.

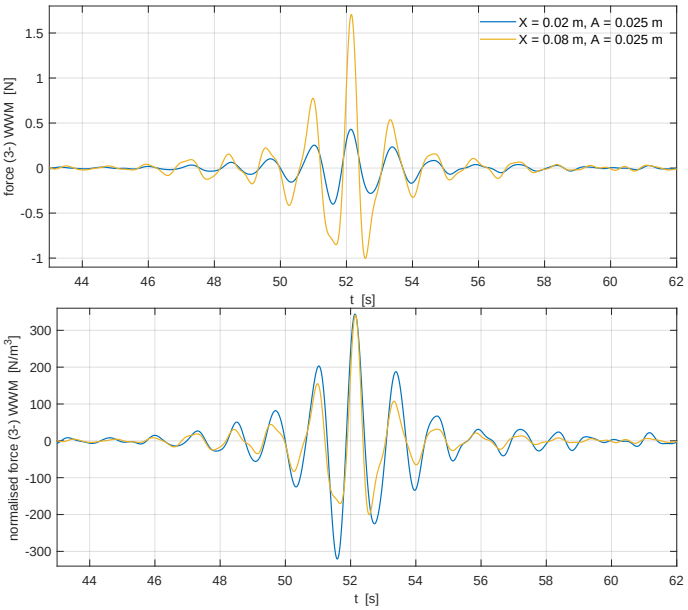

Fig. 9. Extracted third-order $(3-)$ wwm force. Top and bottom plots show the raw and the normalised data respectively.

signals from the diffraction and the radiation runs, which follow from (4) and (5) respectively. Note that in this figure, the colour scheme is not consistent with the rest of the paper - the legend provides the information on the data. The top plot is for the smallest motion amplitude case with $X = 0.02$ m, while the bottom is for the $X = 0.08$ m condition. The signals containing the linear diffraction force (denoted by (1) w) from the combined and the diffraction runs are in good agreement in the smallest motion case, suggesting that the $(3-)$ wmm cross-terms are negligible. In the larger motion case, however, the force in the combined test is considerably lower (while the diffraction test data is the same in both plots). In the extracted force signals containing the linear radiation force (denoted by (1) m), we note differences in the combined and the pure radiation runs at both motion amplitudes.

Subtracting the processed radiation-run first-harmonic force signals from the analogous combined-run signals, allows us to isolate the $(3-)$ wwm terms. These are displayed in the top plot in Fig. 9. We can then test whether these differences scale linearly with motion and quadratically with incident waves. We note, however, that the wave conditions are not varied here, so that dependence is not relevant. The normalised curves are displayed in the bottom plot in Fig. 9, where a reasonable collapse can be seen. In the absence of the force measurements in the radiation tests with $X = 0.05$ m, only two curves are available. We also note that the $(3-)$ wwm force in the smallest amplitude case is really rather small (< 0.5 N), and thus subject to high noise-to-signal ratio, especially considering that this time series is obtained from six independent tests.

We can analyse the free surface measurements in an analogous way. The extracted $(3-)$ wwm wave signals are displayed in Fig. 10, where a reasonable agreement in the normalised curves can be seen. We are faced with a similar difficulty with respect to the magnitude of the $(3-)$ signals, as these are only $O(1)$ mm, so close to the wave gauge sensing precision. Despite this, the observed nonlinear trends in the first-harmonic force and free surface derived from the combined experiments, suggest third-order interaction terms as a plausible mechanism.

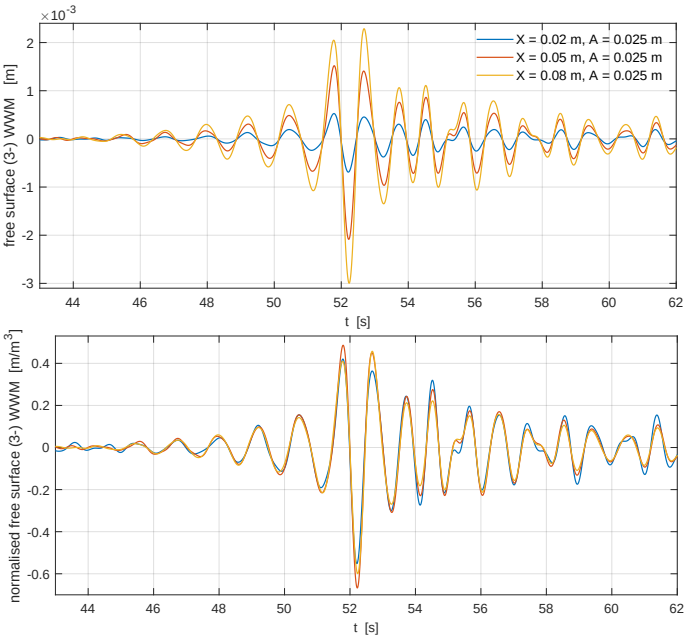

Fig. 10. Extracted third-order $(3-)$ wwm free surface. Top and bottom plots show the raw and the normalised data respectively.

We have noted above that one cannot account for the nonlinear changes of the first-harmonic quantities by simply adopting appropriately modified frequency-domain coefficients. In the absence of a full third-order theory, approximations are sought. Chen *et al.* [9] propose a simplified description of nonlinear diffraction forces on fixed vertical cylinders, whereby the higher-

order forces are calculated from powers of the linear signals and its Hilbert transform. Following [12], we note that the $(3-)$ components could thus be approximated via

$$A^3 f^{(3-)} \cos(\phi + \theta^{(3-)}) \approx (x_L^2 + x_{LH}^2)(\alpha x_L + \beta x_{LH}), \tag{6}$$

where x_L denotes the linear signal and x_{LH} its Hilbert transform. The first term on the right-hand side represents a square of the envelope of the linear signal, while the second term is a scaled and potentially phase-shifted variant of the linear quantity. It is clear how the right-hand side represents a first-harmonic quantity which is rather localised in time (compared to the linear signal) due to the envelope squared multiplier. Without dwelling too much on the details of the underlying theory related to (6), we note that its application is straightforward as it simply entails calculations of simple powers of linear signals.

For the $(3-)$ mmm terms, the appropriate linear signals could be the (linear) body motion, which here is imposed and given by $X\cos\psi = X\cos(\omega t + p_m)$. Alternatively, one could use the linear radiated free surface or the linear radiation force, both given by $X f_m \cos(\psi + \theta_m)$, where the (f_m, θ_m) are the displacement-to-wave and displacement-to-force transfer functions respectively. Fig. 11 shows the approximations as per (6) for the radiated force components in phase with the body acceleration and velocity, where the displacement has been used for the linear signals x_L and the coefficients α and β follow from a simple least-square fit. The agreement is by no means perfect, but the simplicity of the proposed approach lends itself to further investigation. In time-domain models of WEC dynamics such additional (3-) forcing terms could be easily incorporated, as they rely only on known linear quantities. Thanks to the novel experiments with controlled motions and the signal processing of the measurements, one can isolate all the different (3-) terms and attempt to account for their effects in numerical models. This remains as further work, together with thorough validation of our hypothesis that the observed nonlinearities are indeed third-order potential flow effects.

V. Conclusions

This paper introduces a large experimental campaign of a heaving spherical buoy comprised of radiation, diffraction and combined tests, designed for a detailed investigation of nonlinear hydrodynamic effects. To this end, the body motions in the experiments are fully controlled, allowing for independent variation of the incident wave conditions and the imposed motions. Judicious combinations of recordings from the different phase- and amplitude-manipulated tests, enable isolation of different linear and high-order responses.

We focus our analysis on the first-harmonic frequency range, which is of most relevance to wave energy converters. By examining multiple radiation runs with progressively increasing driving motion amplitudes, we observe nonlinear changes to the added mass and radiation damping force coefficients, as well as the radiated free surface. For the spherical body investigated here, as the motion oscillations increase, its wave-generating ability is found to reduce while the hydrodynamic force components in phase with the body acceleration are seen to increase. These nonlinear effects would directly influence the WEC operation. We also analyse the same actuated tests with incident waves present, and describe a methodology for isolating various nonlinear cross-terms. Thanks to tests performed at different excitation amplitudes, for both waves and motion, we can explicitly identify the dependence of the various nonlinear terms on the input amplitudes. The findings prompt us to explain the observed nonlinearities as third-order $(++-)$ potential flow effects.

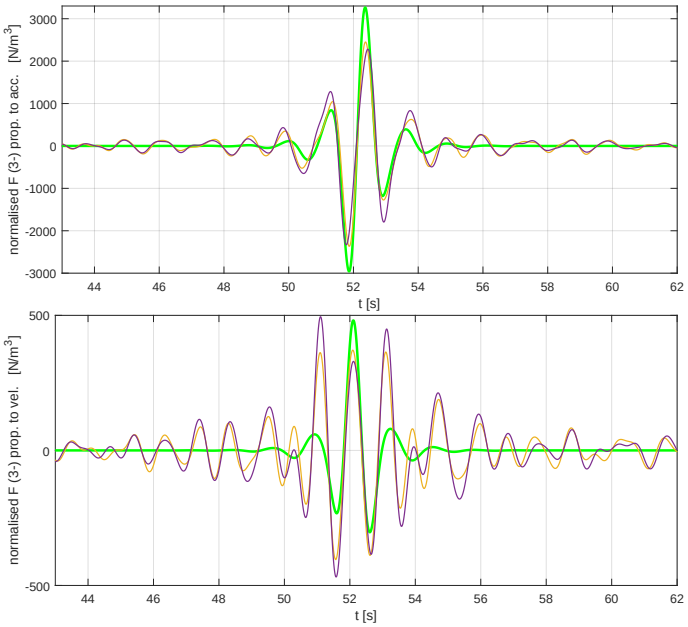

Fig. 11. Extracted normalised $(3-)$ mmm radiation force components in phase with body acceleration (top) and in phase with body velocity (bottom). The green curves are approximation as per 6.

Acknowledgement

The authors acknowledge the Australian Research Council Linkage Project LP210100397, the Research Impact Grant from the University of Western Australia (UWA) and the financial support of the Blue Economy Cooperative Research Centre CRC-20180101, established and supported under the Australian Government's Cooperative Research Centres Program. H. Wolgamot is supported by the Australian Research Council Early Career Fellowship DE200101478. A. Kurniawan is supported by Marine Energy Research Australia (MERA), jointly funded by UWA and the Western Australian Government, via the Department of Primary Industries and Regional Development. B. Tan is supported by the Australian Government Research Training Program Fees Offset and the Australian Government Research Training Program Stipend.

References

[1] J. N. Newman, "The second-order wave force on a vertical cylinder," *Journal of Fluid mechanics*, vol. 320, pp. 417–443, 1996.

[2] I. Bayati, J. Jonkman, A. Robertson, and A. Platt, "The effects of second-order hydrodynamics on a semisubmersible floating offshore wind turbine," in *Journal of Physics: Conference Series*, vol. 524, no. 1. IOP Publishing, 2014, p. 012094.
[3] P. Madsen and D. Fuhrman, "Third-order theory for multi-directional irregular waves," *Journal of Fluid Mechanics*, vol. 698, p. 304–334, 2012.
[4] J. Orszaghova, P. H. Taylor, H. A. Wolgamot, F. J. Madsen, A. M. Pegalajar-Jurado, and H. Bredmose, "Wave- and drag-driven subharmonic responses of a floating wind turbine," *Journal of Fluid Mechanics*, vol. 929, 2021.
[5] O. M. Faltinsen, J. N. Newman, and T. Vinje, "Nonlinear wave loads on a slender vertical cylinder," *Journal of Fluid Mechanics*, vol. 289, p. 179–198, 1995.
[6] M.-H. Kim and D. K. P. Yue, "The complete second-order diffraction solution for an axisymmetric body part 1. monochromatic incident waves," *Journal of Fluid Mechanics*, vol. 200, p. 235–264, 1989.
[7] ——, "The complete second-order diffraction solution for an axisymmetric body part 2. bichromatic incident waves and body motions," *Journal of Fluid Mechanics*, vol. 211, p. 557–593, 1990.
[8] H. Wolgamot, J. Orszaghova, A. Kurniawan, P. Taylor, and J. H. Todalshaug, "Phase-manipulation with multiple controlled inputs to enhance investigation of nonlinear hydrodynamic effects," in *Proceedings of the 38th International Workshop of Water Waves and Floating Bodies*, Ann Arbor, MI, USA, 2023. [Online]. Available: http://www.iwwwfb.org/Abstracts/iwwwfb38/IWWWFB38GLOBAL045.pdf
[9] L. Chen, J. Zang, P. Taylor, L. Sun, G. Morgan, J. Grice, J. Orszaghova, and M. Tello Ruiz, "An experimental decomposition of nonlinear forces on a surface-piercing column: Stokes-type expansions of the force harmonics," *Journal of Fluid Mechanics*, vol. 848, p. 42–77, 2018.
[10] C. Fitzgerald, P. Taylor, R. Eatock Taylor, J. Grice, and J. Zang, "Phase manipulation and the harmonic components of ringing forces on a surface-piercing column," *Proceedings of the Royal Society A-Mathematical Physical and Engineering Sciences*, vol. 470, no. 2168, p. 20130847, 2014.
[11] X. Chen *et al.*, *HydroStar for Experts User Manual*, Bureau Veritas, 2016.
[12] D. Walker, P. Taylor, and R. E. Taylor, "The shape of large surface waves on the open sea and the Draupner New Year wave," *Applied Ocean Research*, vol. 26, no. 3, pp. 73–83, 2004. [Online]. Available: https://www.sciencedirect.com/science/article/pii/S0141118705000052